Cement and Concrete Research 83 (2016) 131–139

Contents lists available at ScienceDirect

Cement and Concrete Research

journal homepage: www.elsevier.com/locate/cemconres

Investigation of early hydration dynamics and microstructural development in ordinary Portland cement using ^{1}H NMR relaxometry and isothermal calorimetry

M.W. Bligh [a,b], M.N. d'Eurydice [c], R.R. Lloyd [d], C.H. Arns [c], T.D. Waite [a,b,*]

[a] School of Civil and Environmental Engineering, The University of New South Wales, Sydney 2052, Australia
[b] UNSW Water Research Centre, The University of New South Wales, Sydney 2052, Australia
[c] School of Petroleum Engineering, The University of New South Wales, Sydney 2033, Australia
[d] Boral Limited, Sydney 2148, Australia

ARTICLE INFO

Article history:
Received 6 September 2015
Accepted 22 January 2016
Available online 2 March 2016

Keywords:
Hydration (A)
Kinetics (A)
Retardation (A)
Hydration products (A)
1H NMR relaxometry

ABSTRACT

Benchtop ^{1}H NMR relaxometry was used to measure the fine temporal resolution of microstructural development during the early hydration of ordinary Portland cement under different levels of retardation. Isothermal calorimetry was used to correlate the various distinct events in water transformation with the progress of hydration reactions. The low field (2 MHz) NMR technique used in this study detected signals from only the mobile water contained in the capillary and gel pores with water incorporation into hydration products highly correlated with heat production, including the reproduction of subtle features. Following the induction period, an initial T_2 decline period, which encompassed the acceleration period of hydration, was characterized by incorporation of water into hydration products without any associated gel pore formation. Gel pore formation commenced at the peak in hydration rate, indicating a change in the morphology of C–S–H growth. All the observed features of microstructural development were preserved under retardation.

1. Introduction

Development of microstructure during the early hydration of Ordinary Portland Cement (OPC) has attracted interest both due to the importance of microstructure to emergent bulk properties and to the advancements in analytical tools and techniques suitable for probing this complex evolving system [1,2]. The apparent potential for influencing microstructure development by controlling hydration reactions has created particular interest in links between the two processes, however, these links, and the scale of microstructure (including molecular structure) at which investigations should optimally focus, remain elusive and are lacking in mechanism-based analysis [3].

Non-invasive methods of continuously monitoring reactions and changes in hydrating cement are highly attractive for obvious reasons. Detection of the state of hydrogen protons, and discrimination and quantification of their various populations, has proved to be a highly fruitful approach since 1) all hydrogen protons in the system originate from added water, 2) water is a key player in hydration reactions, and 3) the state of any hydrogen proton is a function of its chemical and physical environment including microstructure. A number of techniques have been used successfully to probe the state of water in hydrating cement including broadband dielectric spectroscopy (BDS) [7,8], quasi-elastic neutron scattering (QENS) [9,10], and nuclear magnetic resonance (NMR) [11–13]. ^{1}H NMR relaxometry has proved to be a powerful technique that is relatively easy to implement, especially with the development of bench-top instruments capable of rapid analysis of large samples.

In combination with the development of a robust conceptual model for the microstructure of C–S–H gel [14–16], significant advances have been achieved over the last decade in the design of ^{1}H NMR relaxometry experiments, the interpretation of data, and the identification of discrete proton populations associated with proposed microstructural features [17–20]. Using quadrature (solid) echo and Carr–Purcell–Meiboom–Gill CPMG (spin) echo techniques in combination, Muller et al. [21] identified four key populations of hydrogen protons in hydrating white cement: 1) hydrogen protons associated with the minerals ettringite and portlandite, 2) C–S–H interlayer water, 3) gel pore water associated with the small interstices between C–S–H globules, and 4) capillary pore water initially associated with the space between the cement grains and, later, as inter-hydrate spaces. Of these four populations, identification of the C–S–H interlayer water is probably least resolved, likely due to the presence of both chemically and physically bound water [12]. Also, bench-top NMR instruments are often limited to a minimum echo time in the vicinity of 100 μs, which is the same as

* Corresponding author at: School of Civil and Environmental Engineering, The University of New South Wales, Sydney 2052, Australia. Tel.: +612 9385 5060.
E-mail address: d.waite@unsw.edu.au (T.D. Waite).

http://dx.doi.org/10.1016/j.cemconres.2016.01.007

that reported for the position of the T_2 (transverse relaxation time) peak associated with C–S–H interlayer water [11,21]. Information regarding the populations of low-mobility hydrogen protons with extremely fast relaxation times has only been achieved using white cements, free from paramagnetic impurities.

The impact of routinely used and cost effective admixtures on cement hydration processes linked to microstructural development has received limited attention. High levels of sucrose have been shown to have an impact on pore structure and spatial distribution of hydrates, suggested to be due to enhanced homogeneous nucleation of C–S–H in the pore space away from the cement grains [4]. More recently, synchrotron-based XRD enhanced microtomography has been used to reveal a profound effect of superplasticizers on the distribution of C–S–H in hydrated OPC. In the absence of superplasticizer, C–S–H distribution was highly correlated with that of the cement grains, while in the presence of superplasticizer, the C–S–H distribution was random with homogeneous nucleation of C–S–H apparently occurring in the pore spaces [5]. A greater extent of homogeneous nucleation might be expected to lead to a more uniform microstructure with less capillary porosity and a higher specific surface area [6], with implications for mechanical bulk properties and permeability.

In this study we have monitored, with high temporal resolution, early hydration of OPC with and without retardant using bench-top ^{1}H NMR relaxometry and isothermal calorimetry with the aim of 1) determining which populations of water are measurable by bench-top NMR in hydrating OPC and how their dynamics relate to heat output from hydration reactions, and 2) investigating whether retardation of early hydration reactions impacts on the dynamics of water populations, and associated microstructure, in a measurable manner that suggests an evolution towards an altered microstructure, such as more homogeneous C–S–H distribution, with implications for resultant bulk properties.

2. Materials and methods

2.1. Materials

Ordinary Portland cement (OPC) was obtained from Boral Limited, Australia. The elemental analysis is shown in Table 1. Citrate was prepared as a 10% solution of sodium citrate (trisodium citrate dihydrate, Chem Lab). A commercial retardant commonly used in concrete manufacture (Retarder N, Sika; recommended typical dosage of 2 ± 1 mLkg^{-1}) containing selected carbohydrates in liquid form was also used in investigations. All solutions were made using MilliQ (MQ, Millipore) water (>18 MΩ cm). MQ water was used in the production of cement paste.

2.2. Methods

All investigations used cement pastes mixed at a water-to-cement ratio of 0.45. Retardant solutions were added to mixing water in the desired proportions. Retarder N was added on a volume per weight of cement basis (mL kg^{-1}), while citrate was added on a weight per weight of cement basis (g kg^{-1}). Pastes were produced by adding cement to mixing water in a plastic beaker and stirring vigorously with a spatula by hand for two minutes. Excellent reproducibility of the mixing, at least with regards to the progression of hydration, was confirmed from calorimetry analyses (data not shown). For NMR experiments, paste was mixed and immediately poured into a 45 mL styrene vial sealed with a screw top lid, which was then inserted into the instrument bore to commence measurements. For calorimetry, 7 g of mixed cement paste was weighed into a glass vial (2 replicates), crimp sealed and inserted into the instrument.

Table 1
Main elemental composition of investigated OPC.

Oxide	Weight %
CaO	64.56
SiO2	20.09
Al2O3	5.38
Fe2O3	2.96
SO3	2.67
MgO	1.22

Transverse relaxation times (T_2) for hydrating cement were measured using a Carr–Purcell–Meiboom–Gill (CPMG) pulse sequence [22,23] in a Magritek Rock Core Analyser operating at 2 MHz. For each CPMG dataset, 2000 echoes were acquired with an echo time of 105 μs, resulting in a total relaxation delay of 210 ms. Temperature within the magnet bore was maintained at 23 °C throughout the period of measurement. Measurements commenced immediately after sample insertion and were undertaken every 20 min for up to 80 h without disturbing the sample. T_2 distributions were generated via an inverse Laplace transform (ILT) using an exponential kernel [24,25] where the regularization parameter α was optimized according to the L-Curve analysis [26] of the data for intermediate hydration times. Log-normal fits were used to deconvolute the distributions and discriminate the contributions from two hydrogen proton populations: 1) T_2L—long relaxation times, and 2) T_2S—short relaxation times (Fig. 1). The total amount of liquid water in the system was quantified at the start of the experiment from the amplitude of the ILT multi-exponential fitting curve at the time of the first echo. Consumption of 'measurable' water as hydration progressed was monitored using this metric. The weight of the sealed vial containing added cement and water was measured at the start and end of the experiment in order to confirm that no water was lost from the system due to evaporation. The contributions of both populations to the total signal were determined from the individual fitted distributions by reconstructing individual echo decays. Hence, the amplitude of the reconstructed first echo was compared to the measured first echo to confirm the validity of the technique. In order to reduce noise, a Gaussian low-pass filter, with a standard deviation of 80 min (4 experimental points), was applied to the series of first echo amplitudes as a function of the curing time. The applied filter was effective in removing high frequency fluctuations while revealing low frequency features of interest and facilitating useful derivative plots that required no additional smoothing (see Supplementary Material, Fig. S1 and animation).

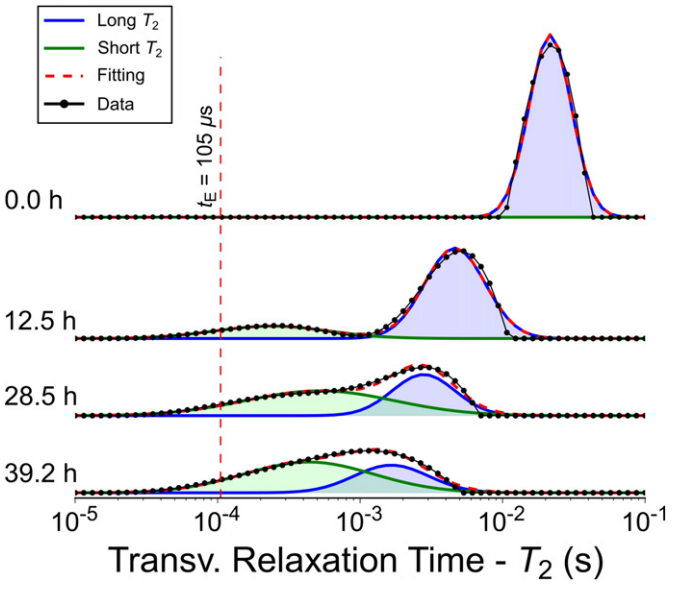

Fig. 1. Examples of log-normal fits of T_2 distributions following Laplace inversions of echo decays from hydrating OPC with no retardant. The vertical dashed line shows the minimum echo time of the instrument.

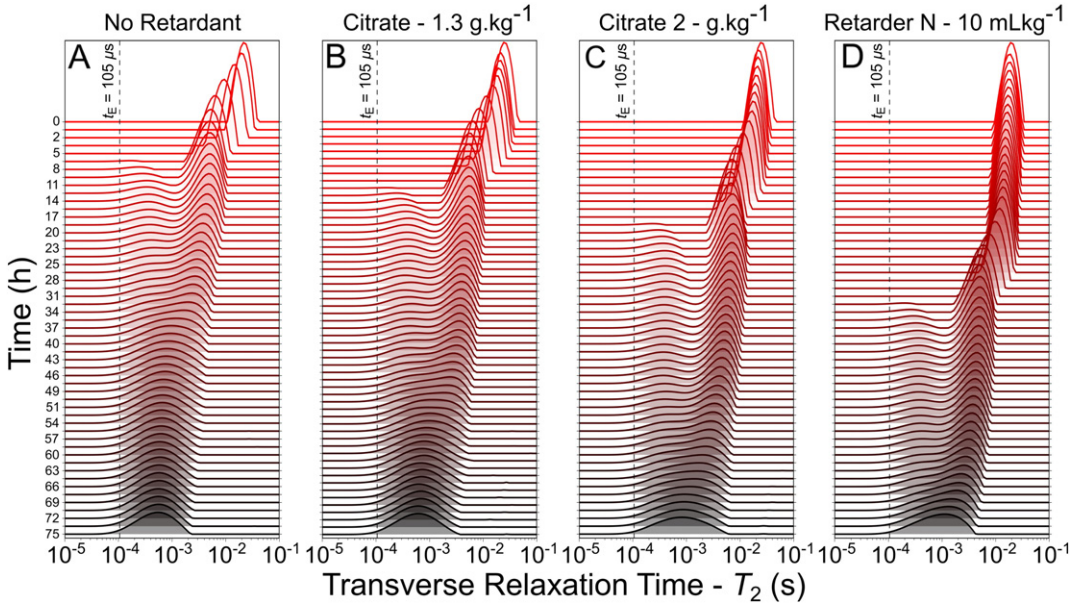

Fig. 2. Evolution of T_2 distribution during hydration of OPC with A) no retardant, B) 1.3 g kg^{-1} citrate, C) 2 g kg^{-1} citrate, or D) 10 $mLkg^{-1}$ Retarder N. The vertical dashed lines show the minmal echo time of the instrument.

An eight-channel TAM Air calorimeter (TA Instruments) was used to monitor the isothermal heat production from hydrating cement paste at 23 °C. A time lag existed between the contact of water and cement and the start of measurement due to time for mixing (2 min), sample weighing into the glass ampoule, and stabilization of the block temperature (typically 45 min).

3. Results and discussion

3.1. T_2 distributions and the meaning of the T_2L and T_2S peaks

The development of multimodal distributions of T_2 values (Fig. 2) during early cement hydration is an established feature of ^{1}H NMR relaxometry and there is general consensus that the discrete peaks are representative of water confined in different structural levels within the cement [17,20,27–29]. Various authors have developed schemes, with much commonality between them, for the assignment of T_2 peaks to separate structural elements [e.g. 11, 21]. T_2 values in the millisecond range (T_2L) are attributed to water in capillary pores, which initially is interstitial water between the clinker grains but then evolves to become inter-hydrate water with pores of about 10 nm. In comparison, T_2 values in the hundreds of microseconds range (T_2S) are attributed to water in gel pores of about 3 nm, conceptualized as existing between the gel globules that comprise C–S–H [21]. The validity of this assignment scheme for our system will be considered later in Sections 3.3 and 3.7. The key hydrogen proton populations to which added water is proposed to convert during the early hydration of OPC are shown schematically in Fig. 3.

The shapes of the T_2L and T_2S peaks were in part determined by the value of the regularization parameter α used in the Laplace inversions of the signal decays. Higher values of α lead to smoother and more stable solutions, although broad with lower resolution. On the other hand, low values of α provide high resolution but with instability. Due to the high temporal resolution of measurements, smooth transition between time points is expected and random shifts of T_2 peak positions indicate a suboptimal value of α. The value of α was chosen based on the L-Curve analysis [26] such that the temporal evolution of peak positions and shapes were smooth. Hence, narrow distributions, such as those presented in some studies (e.g., Muller et al. [21]), were not achievable under the requirement of smooth transitions between time points.

3.2. Overall trends and patterns

Upon the commencement of measurements, following the addition of water (plus retardant) and mixing of paste, the water within the

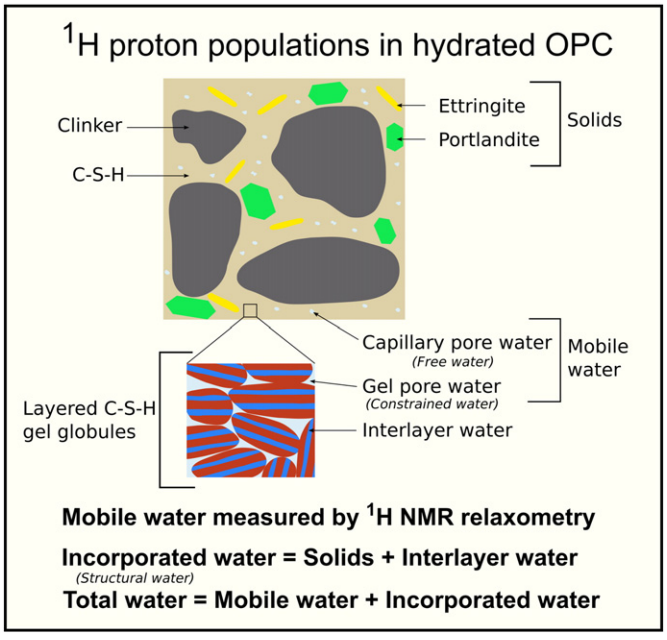

Fig. 3. Simple scheme for OPC, following the early hydration, illustrating the discrete populations of hydrogen protons resulting from the transformation of added water and the formation of hydration products. The C–S–H gel structure is based on the colloid model [15,16]. Only the mobile water, comprising capillary and gel pore water, was able to be measured by the NMR instrument. Therefore, by measuring the total water at the start of the experiment, when incorporated water (IW) equals zero, IW at any time was measured as the decrease in mobile water. The hydrogen proton populations discriminated in QENS analysis [9], structural, constrained, and free water (shown in parentheses), correlate broadly with incorporated water, gel pore water, and capillary water respectively.

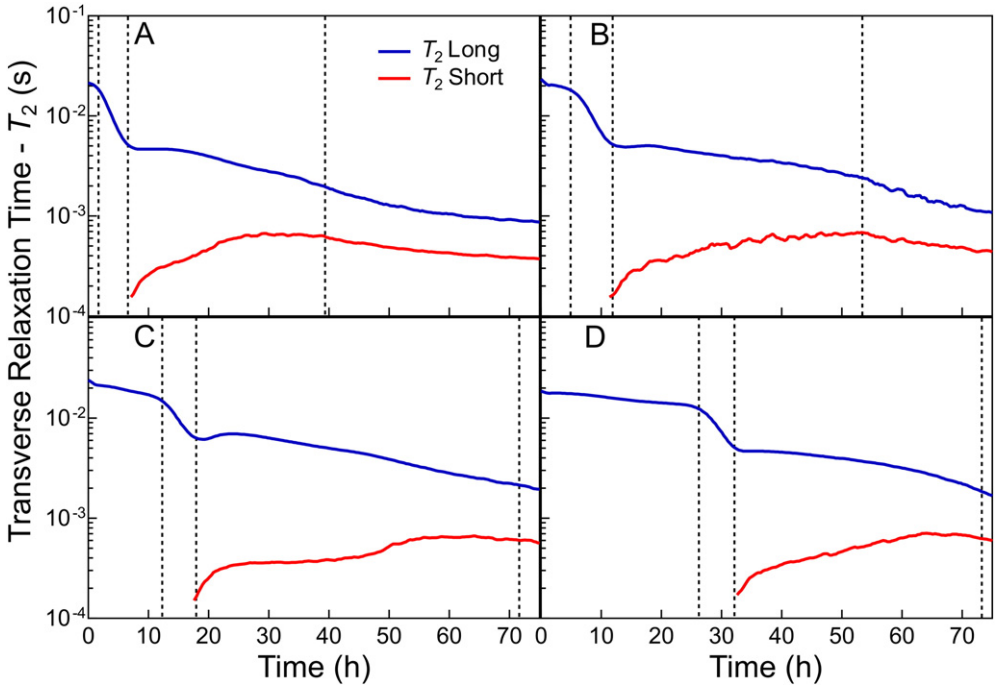

Fig. 4. Positions of fitted peaks of the T_2 distributions (shown in Fig. 2) during hydration of OPC with A) no retardant, B) 1.3 g kg^{-1} citrate, C) 2 g kg^{-1} citrate, or D) 10 mLkg^{-1} Retarder N. Vertical dashed lines show the times t_1, t_2, and t_3 that show the beginning of the ITD, gel pore formation, and C–S–H densification periods respectively.

interstices between the clinker grains produced a well-defined T_2 peak (T_2L) positioned at ~20 ms that slowly shifted to lower values of T_2 during the induction period before shifting rapidly to T_2 values approximately an order magnitude lower (Fig. 4). This period of rapid decrease in T_2 is termed here the 'Initial T_2 Decline' (ITD). The appearance of a second peak at lower T_2 values (T_2S) following the ITD signified the commencement of gel pore formation. As hydration proceeded, the signal associated with the T_2L peak decreased while that associated with the T_2S peak increased (Fig. 5), indicating that capillary pore space was decreasing while gel pore space was increasing. This trend was broadly interpreted as indicating that capillary pore space was being replaced by hydrates containing gel pore space. Gel pore formation ceased approximately 30 to 40 h after commencing and, at the same time, capillary pore water content stabilized (Fig. 5).

The progress of early hydration, both in the absence and presence of retardant, was characterized by four phases: 1) induction period, 2) ITD, 3) gel pore formation, and 4) C–S–H densification (Fig. 5).

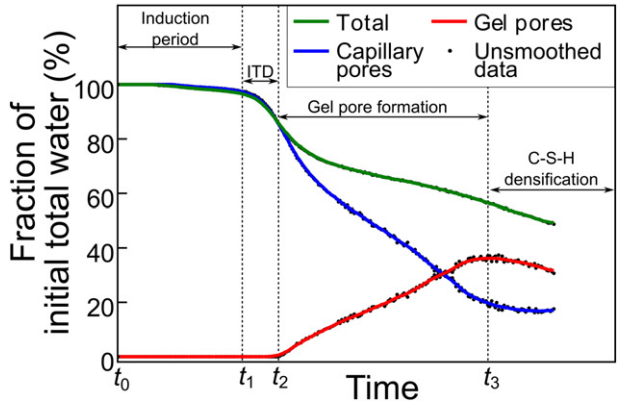

Fig. 5. Data for the Retarder N treatment resulting from the ILT and peak fitting procedures, before and after the application of a Gaussian filter, illustrate 1) the effect of this smoothing operation and 2) the proposed phases of early hydration that are clearly delineated by distinct events. t_1—Induction period ends with the start of water consumption and the start of the initial T_2 decline (ITD). t_2—The ITD ends and gel pore formation commences. t_3—Gel pore formation ends and C–S–H densification commences.

These phases are delineated by distinct time points; each signifying a change in the system. The end of the induction period (t_1) is marked by rapid acceleration in hydration, measured as the decrease in total measurable water, and the start of the ITD. The end of the ITD (t_2) coincides with the peak in hydration rate and the start of gel pore formation which stops (t_3) at the same time as T_2L and T_2S peaks merge to produce an apparently monomodal distribution (Fig. 2) and the position of T_2S peak starts to shift to lower T_2 values.

3.3. Meaning of measurable water

Water detected by the CPMG experiment must be sufficiently mobile such that interactions with the pore surfaces result in a transverse relaxation long enough to produce an echo signal following the first refocussing pulse. The decay times of hydrogen protons associated with chemically reacted water, such as that incorporated into the minerals ettringite and portlandite, are too short and the magnetization from these crystalline structures cannot be refocused with an 180° pulse. For this reason, these contributions are lost in the CPMG experiment as hydration proceeds. Furthermore, any relaxation component shorter than the echo time (105 μs) are also lost due to both the electronic limitations of the low field benchtop instruments and the magnetic inhomogeneity resulting from high levels of paramagnetic impurities in the OPC samples [20]. Water that has been incorporated into the C–S–H gel as interlayer water also appears to be not measured by our instrument, although this is less conclusive than for the mineral forms and will be discussed further below in Section 3.4.

Hydration was characterized by a continual decrease in measurable water (Fig. 6), noting that no water loss due to evaporation was measured at the end of hydration. Water that has become unmeasurable due to reduced mobility resulting from incorporation into hydration products will be termed here as 'incorporated water' (IW). Also, we propose that the fraction of the initial total measureable water represented by incorporated water (IW%) is a measure of hydration degree. We also propose that IW comprises water incorporated into the minerals ettringite and portlandite, as well as a third solid component previously identified and proposed to be hydrogen protons contained within the

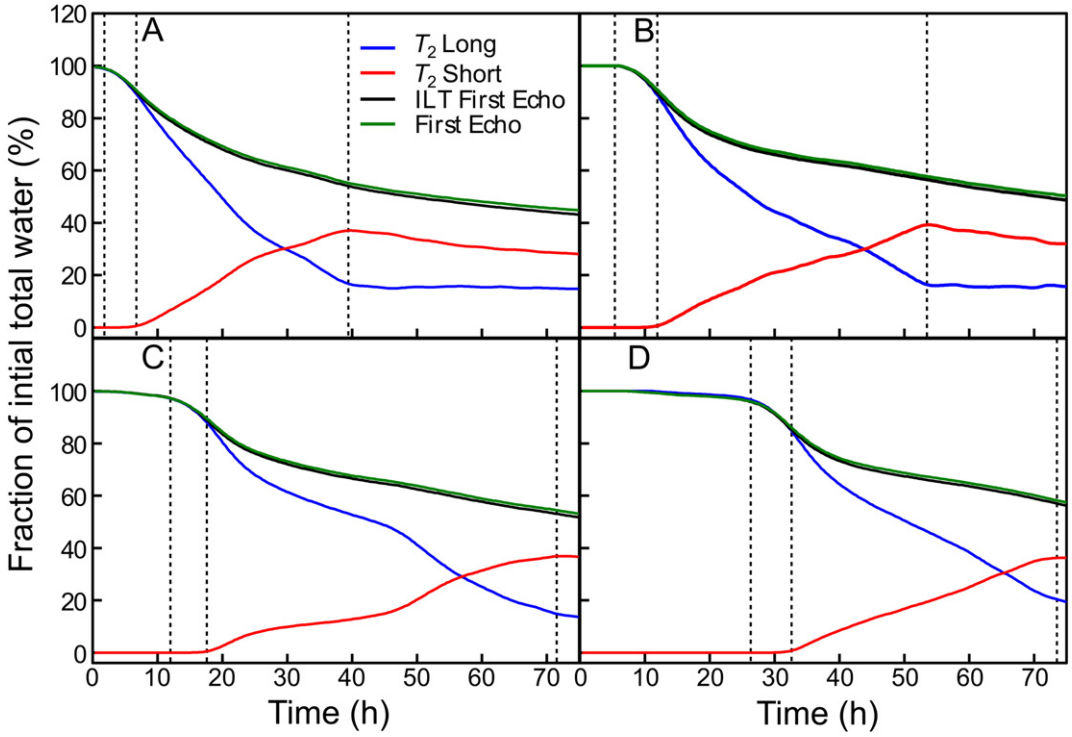

Fig. 6. Mobile water during hydration of OPC with A) no retardant, B) 1.3 g kg^{-1} citrate, C) 2 g kg^{-1} citrate, or D) 10 mLkg^{-1} Retarder N. Water associated with long and short T_2 peaks was calculated as a fraction of the initial total water and assigned to capillary and gel pore water respectively. The total water has been calculated in two ways: 1) from the amplitude of the first echo, and 2) from the amplitude of the first echo that has been reconstructed using the inverse Laplace transformation from sum of the individual peak fits. Vertical dashed lines show the times t_1, t_2, and t_3 that show the beginning of the ITD, gel pore formation, and C–S–H densification periods respectively.

C–S–H layers [17], and C–S–H interlayer water, since it was not possible to distinguish between them.

Interpretation of ^{1}H NMR relaxometry data and assignment of signal components to C–S–H interlayer water have become clearer over recent years, although previous work attempting to quantify interlayer water (and hydrogen protons present in other solid components) has been undertaken using white cement. Generally, interlayer water is considered to be more mobile than water incorporated into the mineral solid components and therefore exhibits higher T_2 values. Two early studies have reported components with T_2 values of 60–100 μs that appear after the start of gel pore formation and are continually produced up to 100 h. The appearance of these signal components has been interpreted as either an expansion of the C–S–H interlayer space [30] or as the change in C–S–H morphology from a fibrillar to a sheet-like structure [11]. Recent series of studies [17–19,21,27–29] provide a clearer picture of the different hydrogen proton populations and their evolution during hydration in white cement. In these studies, interlayer water has been assigned to a component with a T_2 value of ~100 μs that is produced continuously, and broadly in proportion to the production of the solid fraction containing minerals such as ettringite and portlandite, during hydration [21].

3.4. Inclusion of interlayer water in hydration products

Consideration of the conceptual model provided by Muller et al. [21], and their proposed T_2 value of the interlayer water, highlights the uncertainty in our study as to whether interlayer water was being detected or was part of the IW component. Two aspects of the results have led us to conclude that the latter option is correct: 1) the strong correlation between the rate of IW formation and the rate of heat production, as measured by calorimetry (Fig. 7), indicates that the IW fraction accounts for all the water involved in hydration reactions, including the formation of C–S–H (see Section 3.5 for further discussion); and 2) the gel pore component of measurable water, in which the interlayer water would be included if detected, ceases formation and even begins to decrease approximately 40 to 50 h after the start of the acceleration phase of hydration, in line with the behaviour of gel pore water reported by Muller et al. [21]. Based on this reasoning, we will consider that interlayer water is part of IW in further discussion. Furthermore, this discussion will provide additional indirect support to this proposal.

The structure and stoichiometry of C–S–H gel have been the subject of intense study over the previous decades with the location and state of water within the hydrate being of particular interest [16,31,32]. Water is considered as part of the C–S–H structure, and equivalent to chemically bound water [31], although the water appears to be bound with varying degrees of strength and is liberated progressively over a large range of drying conditions. Most uncertainty exists around physically confined water associated with C–S–H designated as interlayer water in the Colloidal-Model-II of C–S–H [15]. Hence, there is some uncertainty within the literature regarding the chemical and physical status of this interlayer water and its role in heat producing hydration reactions.

Quasi-elastic neutron scattering (QENS) studies of early cement hydration support the proposal that interlayer water participates in heat producing reactions. Refining an earlier approach [33], Thomas et al. [9] decomposed the mobile water signal into free and constrained water fractions, and combined constrained water with structural (solid) water fractions to form a bound water index (BWI). While the BWI was able to be fitted well with a hydration model [34], structural water alone correlated to heat production during cement hydration and formation of constrained water ceased after ~1 day despite continuation of hydration [9]. These authors concluded that structural water in C–S–H included both chemically bound and interlayer water and that constrained water included water in the smallest of gel pores and adsorbed to solid–pore interfaces. Constrained water was contended to be solely associated with high surface area, low density (LD) C–S–H (LD C–S–H), while both LD (low density) and HD (high density) C–S–H contain structural water. Despite an uncertain role of constrained water in early hydration, the conceptual model of interlayer

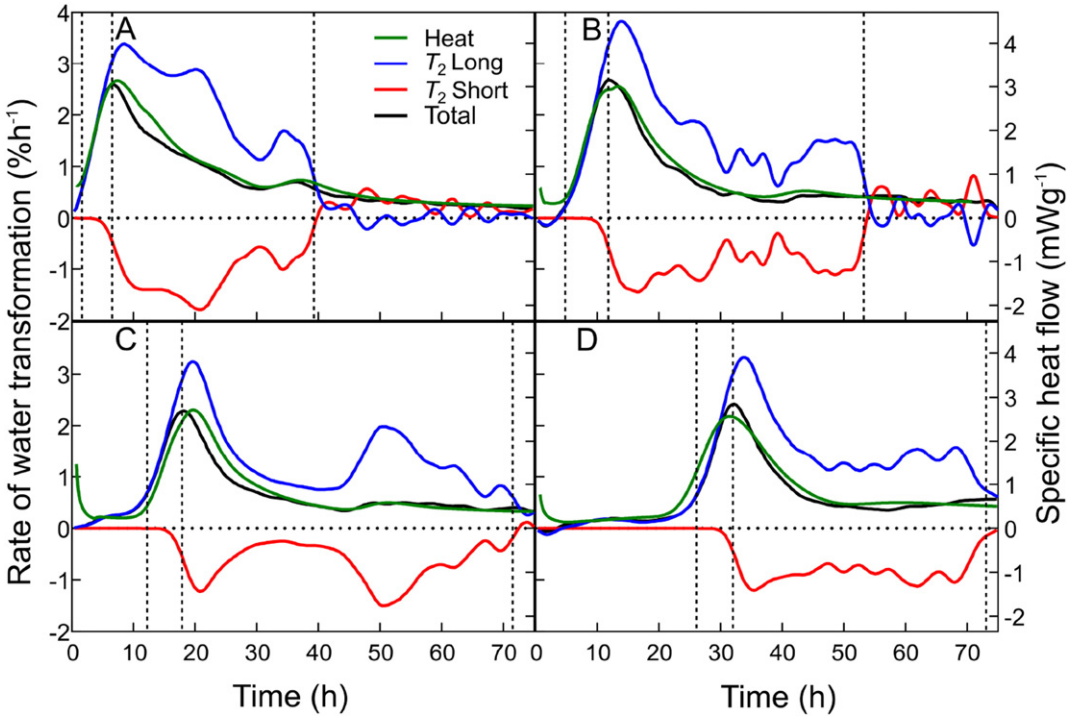

Fig. 7. Rates of water transformation, calculated as the negative derivatives of the measurable water plots, compared to the rate of heat production measured by isothermal calorimetry for A) no retardant, B) 1.3 g kg^{-1} citrate, C) 2 g kg^{-1} citrate, or D) 10 mLkg^{-1} Retarder N. Note that the total rate of water transformation is equivalent to the rate of IW production. Vertical dashed lines show the times t_1, t_2, and t_3 that show the beginning of the ITD, gel pore formation, and C–S–H densification periods respectively.

water developed by these QENS studies tends to support our proposal that IW includes interlayer water and that the formation of interlayer water is part of the heat producing hydration reactions. The inclusion of gel pore water in the BWI during the main hydration peak highlights the close connection between hydrate formation and gel pore formation. The correlations between the populations identified using QENS and those proposed in this study are illustrated in Fig. 3.

Other studies have included water with greater mobility than interlayer water in hydration reactions [35,36] and excluded interlayer water from reactions [37], using differential scanning calorimetry and the T_1 signal amplitude from ^{1}H NMR relaxometry respectively.

In studies where XRD was used to quantify the consumption and formation of different phases during hydration of alite [38] and cement [39], the relationships between enthalpy of reaction and water content of the hydration products implied the involvement of interlayer water in heat producing reactions. Using a simple set reactions based on a formulation for C-S-H with a H:Si ratio of 2.6, these XRD measurements enabled theoretical calculation of heat production which matched calorimetric measurements well. This H:Si ratio was well in excess of 1.8, the value recently considered to account for C-S-H associated water, including interlayer water [16].

While it appears that heat production may possibly be correlated with populations of water that both include and exclude interlayer water, on balance the weight of evidence supports the inclusion of interlayer water in heat producing reactions and supports the proposal that it is part of the IW fraction in this study.

3.5. Correlation of rate of incorporated water production with heat flow

The rate of production of IW is very closely correlated in all cases with the rate of heat production as measured by calorimetry (Fig. 7). While in the absence of retardant the rate of IW production drops below that of heat flow during the first part of the deceleration phase (possibly related to C_3A dissolution as discussed further below), the reproduction of the small peak in heat flow at ~37 h is quite notable (Fig. 7A). In the citrate treatments, this feature is still evident in heat flow, as a broad peak around 43 h and 51 h respectively, and again appears to be reproduced in IW production (Fig. 7B and C). Interestingly, these subtle features appear to be accentuated by both the rate of disappearance of capillary pores and the rate of formation of gel pores, which tend to mirror each other. Even in the Retarder N treatment (Fig. 7D), where this small secondary feature has not been detected by either heat flow or IW production measurements, there appears to be a similar pair of mirrored peaks. The relationship between capillary and gel pores, and the possible interpretation of these mirrored peaks will be discussed further in Section 3.7.

The proportionality between the rate of heat production and the rate of IW production was identical for all treatments (note that the same axes were used for all plots), even where high retardation has slowed the reaction rate, further supporting the proposal that the IW fraction represents the water taking part in the heat producing reactions. Also, proportionality was maintained throughout early hydration, suggesting that the amount of heat produced per mole of water consumed (transformed to IW) was constant. Deviation from this proportionality occurred only during the deceleration phase in the absence of retardant where the heat flow was higher than suggested by the water consumption. Two reactions have been suggested to dominate the production of heat prior to sulphate depletion [39]: 1) silicate reaction (Eq. (1)) where C–S–H formation and portlandite precipitation occur synchronously with C_3S dissolution, and 2) ettringite precipitation (Eq. (2)) from ions resulting from initial dissolution of C_3A and calcium sulphates.

$$(CaO)_3.SiO_2 + 3.9H_2O \rightarrow (CaO)_{1.7}.SiO_2.(H_2O)_{2.6} + 1.3Ca(OH)_2 \quad (1)$$

$$6Ca^{2+} + 2Al^{3+} + 3SO_4{}^{2-} + 12OH^- + 26H_2O \rightarrow (CaO)_3.Al_2O_3.(CaSO_4)_3.(H_2O)_{32}(\text{Ettringite}) \quad (2)$$

Ettringite precipitation has been shown to be relatively constant during the main peak of hydration [39], therefore heat production and water consumption are expected to be proportional to the rate of the silicate reaction. Following sulphate depletion, C_3A dissolution also contributes to heat production, however, water will not be transferred to

the IW fraction during this reaction since no solid phase is formed. This decoupling of heat production from IW production during the initial burst of C_3A dissolution could account for higher heat flow per mole of water consumed during this period. The lack of this decoupling where retardant was present likely indicates a change in the aluminate–sulphate balance resulting from effects such as the reactivity of cement phases, the dispersion and wetting of cement grains, and the dissolution rate of calcium sulphates [40].

Based on the rate plots of Fig. 7, the proportionality between water consumption and heat production was calculated as ~17,000 joules per mole of water. This value sits favourably between the calculated values of ~21,000 J mol^{-1} for silicate reaction and ~10,000 J mol^{-1} for ettringite precipitation, using enthalpies of −561 Jg^{-1} and −214 Jg^{-1} for the reactions shown in Eqs. (1) and (2) respectively [39], along with molar weights of 228 and 1255 for C_3S and ettringite respectively. These values imply that the silicate reaction accounted for approximately 76% of the heat production, a value less than that estimated (~80 to 85%) from study of OPC hydration reported by Jansen et al. [39]. It should be noted however that the cement used by Jansen et al. was higher in CaO and SiO_2, lower in Al_2O_3, and reacted more rapidly such that the peak heat flow was >5 mW g^{-1}, suggesting that the silicate reaction may have formed a greater part of the total heat flow than was the case in our study.

3.6. Initial T_2 decline

The ITD forms a distinctive feature of the T_2 distributions (Fig. 4) and appears in all cases, with and without retardant, to immediately precede the start of gel pore formation (Figs. 5 and 6). Importantly, while commencing just after the onset of the acceleration period of hydration, the completion of the ITD coincides exactly with the end of the acceleration period and the hydration peak. Therefore, the profound changes in microstructure occurring during the ITD appear to be closely linked with the processes controlling the rate of hydration.

A large decrease in the T_2 (and T_1) values, usually an order of magnitude, during early hydration is a ubiquitous feature ^{1}H NMR relaxometry studies of cement. A very early study using Portland cement measured both T_1 and T_2 changes during hydration and observed T_2 decline commencing at 10 h but which continued till about 50 h [41], much longer than is the case here. A number of investigators of white cement hydration have reported large declines in the T_2 value of the capillary pores for the initial 100 h [11] and for >100 h [30]. More recent studies have reported initial order of magnitude declines in the T_2 values of the capillary pores over 24 h during the initial hydration of OPC derived endodontic cements [28,29] and of white cement [21]. In the latter study, however, gel pore formation commenced after 2 h of hydration, suggesting differences in the relationship between hydration reactions and microstructural development compared to OPC.

Wang et al. [37] showed that the initial decline in the T_1 value of the capillary pore peak correlated well with penetration depth of a Vicat needle. The end of this decline matched exactly the end of the setting period, while the start of the setting period matched the point of upturn in a plot of $1/T_1$. These findings provide strong support for the idea that the processes involved in the ITD are linked to the percolation characteristics of the solid network. While the links between hydration and attainment of the percolation threshold are complex and difficult to resolve [42], the final setting point, which coincides with the peak in hydration rate, has been hypothesised to be due to percolation of hydration products within the pore spaces [43], based on a colloidal growth model. This model was able to match heat production (through scaling) very well and predicted a peak rate at lower and more realistic degrees of hydration compared to previous modelling. The mode of colloidal growth is also consistent with ^{1}H NMR relaxometry data reported by Bortolotti et al. [17] where clusters of constant composition, comprised of C–S–H gel globules and gel pores, were proposed to fill the capillary pore spaces during hydration.

Concepts and studies regarding percolation and setting indicate that hydration progress during the ITD likely involved the penetration of the spaces between the cement clinker grains, responsible for the initial peak in the T_2 distribution at 20 ms, with diffuse and highly porous C–S–H as proposed by Bishnoi and Scrivener [44]. A later review of hydration models concluded that in-filling of pores occurred via dendritic growth of low density hydrates [45] and TEM micrographs have illustrated the fibrous manner of growth displayed by C–S–H during early hydration [46]. Such growth into the initial pore space will substantially increase the surface area within the pore volume and hence reduce relaxation times but without the formation of a population of pores producing shorter T_2 times of hundreds of microseconds that characterize gel pores. Holly et al. [11] observed the appearance of a water population with a stable T_2 value of 100 μs, assigned to interlayer water, after ~10 h hydration. These authors proposed that this event signified a change in growth morphology from a fibrillar to a sheet-like structure.

The cause of the rate peak has been hypothesised to be due to the impingement of hydration products where a low density form of C–S–H ramifies the pore space and later densifies [43–45] with this mechanism compatible with our observation that the rate peak coincides with a change in C–S–H growth morphology. However, a recent paper [47] based on modelling of the hydration processes has proposed that the rate peak is due to a reduction in C_3S dissolution rate due to surface coverage by C–S–H. Furthermore, this mechanism accounts for the insensitivity of early hydration kinetics to the w/c ratio of the cement paste. A possible link between this proposed mechanism and the change in microstructural evolution observed here is unclear.

Based on these observations, we propose that the space between cement grains is rapidly penetrated by very low density fibrillar growth during the ITD with this process providing sufficient additional surface area to decrease T_2 relaxation times by an order of magnitude. After 5 to 7 h the ITD ends, marking a significant change in the system that apparently coincides with the point of final setting, a change in C–S–H growth morphology, and the start of formation of gel pores which are associated with layered C–S–H gel globules. The presence of retardants, while delaying the start of the ITD had only a small apparent effect on the measured characteristics of the ITD; the duration of the ITD was extended from ~5 h with no retardant to ~7 h in the presence of retardants.

3.7. Gel pore formation

The start of gel pore formation coincides exactly with the end of the ITD and the peak in hydration rate (Fig. 6) and, based on the discussion in Section 3.6, with a change in C–S–H morphology from fibrillar to sheet-like structure. Considered within the context of the Jennings colloid model [15], the initial formation of aggregates of gel globules composed of a layered structure is associated with formation of small gel pore spaces and which together constitute the low density (LD) C–S–H.

The mechanisms responsible for the deceleration in hydration rate likely are closely linked to the process of gel pore formation. Various hypotheses have been put forward for the onset of deceleration, and, recently, numerous (chiefly modelling) studies have concluded that the peak is a direct result of nucleation and growth mechanisms [2,47]. The activation energy of hydration has been shown to remain constant during the main hydration peak indicating that there is no transition in the rate controlling reaction at the hydration peak [48], yet it appears that there is some transition occurring in the growth mechanism of C–S–H.

The distinct cessation of gel pore formation is in accord with a limitation, perhaps spatial, to the growth of LD C–S–H leading to the transition to the growth of high density (HD) C–S–H which contains no gel pore spaces [21]. The degree of hydration, as measured by the IW%, at the end of this period is similar in all treatments (Fig. 8).

A crude measure of the density of the hydration products is the ratio of IW to the sum of IW and the gel pore water. The evolution of this ratio

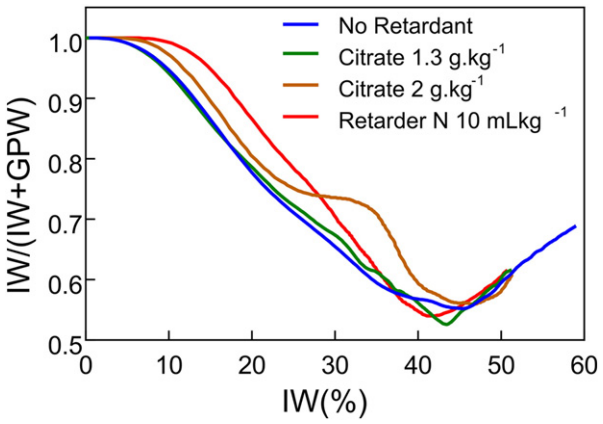

Fig. 8. Ratio of incorporated water (IW) to the sum of IW plus gel pore water (GPW), which together constitute the water associated with hydration products, as function of the degree of hydration expressed in terms of IW%. Until the start of gel pore formation, capillary water is transformed only to IW, then during gel pore formation the ratio declines and reaches a minimum when formation ceases and C–S–H densification commences.

during hydration can be compared between treatments by plotting against IW% as a measure of hydration degree (Fig. 8). Following the induction period and ITD where initial capillary water was transformed to IW without gel pore formation, the ratio declined during the gel pore formation and reached a very similar minimum value for all treatments at the end point of this period. The degree of hydration at which this minimum ratio occurred was also similar, although there was the appearance of a small effect of greater retardation resulting in the minimum occurring at a lower IW%. This effect, while possibly random in nature, might suggest that a denser microstructure could eventuate later during hydration under greater retardation. Nevertheless, all treatments appeared to converge and track an identical path following the start C–S–H densification (Fig. 8).

An intriguing feature can be seen in the plots of changes in water content of capillary and gel pores where the apparent amplification of features in the total water plots occurs (Fig. 7). This is particularly the case in the no retardant treatment at ~21 h and ~35 h and in the 2 g kg^{-1} citrate treatment at ~50 h. The early hydration process, at least until gel pore production ceases, involves the transformation of capillary pores to either 1) hydration products (IW) or 2) gel pore water within the interstices of these hydration products. Hence the rates of IW and gel pore formation are expected to be generally correlated during this period. However, the behaviour illustrated in the plots indicate that the relationship is not constant and that a small increase in hydration rate, relative to the overall trend, is accompanied by a marked increase in the rate of gel pore formation. In the no retardant case (Fig. 7A), the peak at ~21 h is associated with a shoulder region on the deceleration side of the main hydration peak, and the more complex prominent double at peak at ~35 h is associated with the secondary hydration peak. The association with a secondary peak is very prominent at 50 h in the high citrate treatment. Clearly, during these peak periods, the rate at which capillary water is being converted to gel pore water increases substantially compared to the rate of incorporation into hydration products. The following possibilities are suggested by these patterns of behaviour.

1. Changes in structure and density of the of C–S–H product may be occurring due to interactions with new phases, such as sulfoaluminates, that impact growth and/or packing of C–S–H.
2. Measured gel pore water may be a net amount resulting from a dynamic process where gel pore water is continually consumed at the same time as capillary pores are transformed to new gel pores via the production of hydrates. The sudden switch to gel pore water consumption at the end of the gel pore formation period, at least for the two least retarded treatments (Figs. 6 and 7), suggests that this could be the case. As such, the net process becomes negative when gel pore formation ceases while hydration continues. During the above periods of interest, the balance between capillary and gel pore water consumption may change, producing the effect of an increased rate of gel pore production.

4. Conclusions

The key conclusions resulting from this study are as follows.

1. The high correlation between the rate of incorporated water (IW) production and the rate of heat production, where even subtle features such as secondary peaks were reproduced, provides strong evidence that the processes associated with IW production were exothermic.
2. Measurable water was composed of two fractions discerned as long and short T_2 peaks that corresponded well with capillary and gel pore water identified in previous studies using white cement. The cessation of gel pore formation ~40 h after the commencement of hydration provides strong evidence that C–S–H interlayer water was not being measured by the ^{1}H relaxometry method used here. This in turn supports the concept that interlayer water is a product of exothermic hydration reactions.
3. A period of initial T_2 decline (ITD) marked the start of hydration following the induction period and encompassed the acceleration phase of the hydration peak. The formation of hydration products during this period was not associated with the formation of gel pore spaces suggesting a fibrillar growth form of C–S–H, possibly of low density and extending into the pore space causing an order of magnitude decrease in the T_2 relaxation time.
4. Gel pore formation did not commence until the peak of hydration was reached indicating a change in C–S–H morphology in accord with the Jennings colloid model [15] where gel pore space is associated with layered C–S–H gel globules.
5. The presence of retardants appeared to have only minor effects apart from substantial extension of the induction period. The gel pore formation period was somewhat extended and the rate of formation more constant, however, once C–S–H densification was underway, all treatments displayed identical behaviour with respect to hydration degree.

Supplementary data to this article can be found online at http://dx.doi.org/10.1016/j.cemconres.2016.01.007.

Acknowledgments

Financial support for this project has been provided by Boral Limited, Australia.

References

[1] J.W. Bullard, H.M. Jennings, R.A. Livingston, A. Nonat, G.W. Scherer, J.S. Schweitzer, K.L. Scrivener, J.J. Thomas, Mechanisms of cement hydration, Cem. Concr. Res. 41 (2011) 1208–1223.
[2] J.J. Thomas, J.J. Biernacki, J.W. Bullard, S. Bishnoi, J.S. Dolado, G.W. Scherer, A. Luttge, Modeling and simulation of cement hydration kinetics and microstructure development, Cem. Concr. Res. 41 (2011) 1257–1278.
[3] S. Yip, M.P. Short, Multiscale materials modelling at the mesoscale, Nat. Mater. 12 (2013) 774–777.
[4] M.C.G. Juenger, H.M. Jennings, New insights into the effects of sugar on the hydration and microstructure of cement pastes, Cem. Concr. Res. 32 (2002) 393–399.
[5] G. Artioli, L. Valentini, M. Voltolini, M.C. Dalconi, G. Ferrari, V. Russo, Direct imaging of nucleation mechanisms by synchrotron diffraction micro-tomography: superplasticizer-induced change of C–S–H nucleation in cement, Cryst. Growth Des. 15 (2015) 20–23.
[6] J.J. Thomas, H.M. Jennings, J.J. Chen, Influence of nucleation seeding on the hydration mechanisms of tricalcium silicate and cement, J. Phys. Chem. C 113 (2009) 4327–4334.

[7] S. Cerveny, S. Arrese-Igor, J.S. Dolado, J.J. Gaitero, A. Alegría, J. Colmenero, Effect of hydration on the dielectric properties of C–S–H gel, J. Chem. Phys. 134 (2011) 034509.
[8] K.L. Chung, S. Kharkovsky, Monitoring of microwave properties of early-age concrete and mortar specimens, IEEE Trans. Instrum. Meas. 64 (2015) 1196–1203.
[9] J.J. Thomas, S.A. FitzGerald, D.A. Neumann, R.A. Livingston, State of water in hydrating tricalcium silicate and Portland cement pastes as measured by quasi-elastic neutron scattering, J. Am. Ceram. Soc. 84 (2001) 1811–1816.
[10] V.K. Peterson, D.A. Neumann, R.A. Livingston, Hydration of cement: the application of quasielastic and inelastic neutron scattering, Phys. B Condens. Matter 385 (2006) 481–486.
[11] R. Holly, E.J. Reardon, C.M. Hansson, H. Peemoeller, Proton spin–spin relaxation study of the effect of temperature on white cement hydration, J. Am. Ceram. Soc. 90 (2007) 570–577.
[12] P.J. McDonald, V. Rodin, A. Valori, Characterisation of intra- and inter-C–S–H gel pore water in white cement based on an analysis of NMR signal amplitudes as a function of water content, Cem. Concr. Res. 40 (2010) 1656–1663.
[13] P.F. Faure, S. Rodts, Proton NMR relaxation as a probe for setting cement pastes, Magn. Reson. Imaging 26 (2008) 1183–1196.
[14] H.M. Jennings, A model for the microstructure of calcium silicate hydrate in cement paste, Cem. Concr. Res. 30 (2000) 101–116.
[15] H.M. Jennings, Refinements to colloid model of C–S–H in cement: CM-II, Cem. Concr. Res. 38 (2008) 275–289.
[16] A.J. Allen, J.J. Thomas, H.M. Jennings, Composition and density of nanoscale calcium–silicate–hydrate in cement, Nat. Mater. 6 (2007) 311–316.
[17] V. Bortolotti, L. Brizi, R.J.S. Brown, P. Fantazzini, M. Mariani, Nano and sub-nano multiscale porosity formation and other features revealed by 1 H NMR Relaxometry during cement hydration, Langmuir 30 (2014) 10871–10877.
[18] A.C.A. Muller, K.L. Scrivener, A.M. Gajewicz, P.J. McDonald, Use of bench-top NMR to measure the density, composition and desorption isotherm of C–S–H in cement paste, Microporous Mesoporous Mater. 178 (2013) 99–103.
[19] A.C.A. Muller, K.L. Scrivener, J. Skibsted, A.M. Gajewicz, P.J. McDonald, Influence of silica fume on the microstructure of cement pastes: new insights from 1 H NMR relaxometry, Cem. Concr. Res. 74 (2015) 116–125.
[20] A. Valori, P.J. McDonald, K.L. Scrivener, The morphology of C–S–H: lessons from H-1 nuclear magnetic resonance relaxometry, Cem. Concr. Res. 49 (2013) 65–81.
[21] A.C.A. Muller, K.L. Scrivener, A.M. Gajewicz, P.J. McDonald, Densification of C–S–H measured by 1 H NMR relaxometry, J. Phys. Chem. C 117 (2012) 403–412.
[22] H.Y. Carr, E.M. Purcell, Effects of diffusion on free precession in nuclear magnetic resonance experiments, Phys. Rev. 94 (1954) 630–638.
[23] S. Meiboom, D. Gill, Modified spin-echo method for measuring nuclear relaxation times, Rev. Sci. Instrum. 29 (1958) 688–691.
[24] S.W. Provencher, A constrained regularization method for inverting data represented by linear algerbraic or integral-equations, Comput. Phys. Commun. 27 (1982) 213–227.
[25] G.C. Borgia, R.J.S. Brown, P. Fantazzini, Uniform-penalty inversion of multiexponential decay data, J. Magn. Reson. 132 (1998) 65–77.
[26] P.C. Hansen, Analysis of discrete ill-posed problems by means of the L-curve, SIAM Rev. 34 (1992) 561–580.
[27] V. Bortolotti, R.J.S. Brown, P. Fantazzini, M. Mariani, Evolution of a short-T2 liquid-like 1 H signal during the hydration of white Portland cement, Microporous Mesoporous Mater. 178 (2013) 108–112.
[28] V. Bortolotti, P. Fantazzini, R. Mongiorgi, S. Sauro, S. Zanna, Hydration kinetics of cements by time-domain nuclear magnetic resonance: application to Portland-cement-derived endodontic pastes, Cem. Concr. Res. 42 (2012) 577–582.
[29] M. Gombia, V. Bortolotti, B. De Carlo, R. Mongiorgi, S. Zanna, P. Fantazzini, Nanopore structure buildup during endodontic cement hydration studied by time-domain nuclear magnetic resonance of lower and higher mobility H-1, J. Phys. Chem. B 114 (2010) 1767–1774.
[30] J. Greener, H. Peemoeller, C.H. Choi, R. Holly, E.J. Reardon, C.M. Hansson, M.M. Pintar, Monitoring of hydration of white cement paste with proton NMR spin–spin relaxation, J. Am. Ceram. Soc. 83 (2000) 623–627.
[31] R.J.-M. Pellenq, A. Kushima, R. Shahsavari, K.J. Van Vliet, M.J. Buehler, S. Yip, F.-J. Ulm, A realistic molecular model of cement hydrates, Proceedings of the National Academy of Sciences, 2009.
[32] B. Lothenbach, A. Nonat, Calcium silicate hydrates: solid and liquid phase composition, Cem. Concr. Res. (2015).
[33] S.A. FitzGerald, D.A. Neumann, J.J. Rush, D.P. Bentz, R.A. Livingston, In situ quasi-elastic neutron scattering study of the hydration of tricalcium silicate, Chem. Mater. 10 (1998) 397–402.
[34] V.K. Peterson, M.C.G. Juenger, Hydration of tricalcium silicate: effects of $CaCl_2$ and sucrose on reaction kinetics and product formation, Chem. Mater. 18 (2006) 5798–5804.
[35] F. Ridi, E. Fratini, P. Luciani, F. Winnefeld, P. Baglioni, Hydration kinetics of tricalcium silicate by calorimetric methods, J. Colloid Interface Sci. 364 (2011) 118–124.
[36] F. Ridi, P. Luciani, E. Fratini, P. Baglioni, Water confined in cement pastes as a probe of cement microstructure evolution, J. Phys. Chem. B 113 (2009) 3080–3087.
[37] B. Wang, P. Faure, M. Thiéry, V. Baroghel-Bouny, 1 H NMR relaxometry as an indicator of setting and water depletion during cement hydration, Cem. Concr. Res. 45 (2013) 1–14.
[38] S.T. Bergold, F. Goetz-Neunhoeffer, J. Neubauer, Quantitative analysis of C–S–H in hydrating alite pastes by in-situ XRD, Cem. Concr. Res. 53 (2013) 119–126.
[39] D. Jansen, F. Goetz-Neunhoeffer, B. Lothenbach, J. Neubauer, The early hydration of ordinary Portland cement (OPC): an approach comparing measured heat flow with calculated heat flow from QXRD, Cem. Concr. Res. 42 (2012) 134–138.
[40] L.R. Roberts, P.C. Taylor, Understanding Cement–SCM–Admixture Interaction Issues, Concrete International Magazine, January 2007 33–41.
[41] L.J. Schreiner, J.C. Mactavish, L. Miljković, M.M. Pintar, R. Blinc, G. Lahajnar, D. Lasic, L.W. Reeves, NMR line shape-spin–lattice relaxation correlation study of Portland cement hydration, J. Am. Ceram. Soc. 68 (1985) 10–16.
[42] G.W. Scherer, J. Zhang, J.A. Quintanilla, S. Torquato, Hydration and percolation at the setting point, Cem. Concr. Res. 42 (2012) 665–672.
[43] R. González-Teresa, J.S. Dolado, A. Ayuela, J.-C. Gimel, Nanoscale texture development of C–S–H gel: a computational model for nucleation and growth, Appl. Phys. Lett. 103 (2013) 234105.
[44] S. Bishnoi, K.L. Scrivener, Studying nucleation and growth kinetics of alite hydration using mu ic, Cem. Concr. Res. 39 (2009) 849–860.
[45] G.W. Scherer, Models of confined growth, Cem. Concr. Res. 42 (2012) 1252–1260.
[46] E. Gallucci, P. Mathur, K. Scrivener, Microstructural development of early age hydration shells around cement grains, Cem. Concr. Res. 40 (2010) 4–13.
[47] J.W. Bullard, G.W. Scherer, J.J. Thomas, Time dependent driving forces and the kinetics of tricalcium silicate hydration, Cem. Concr. Res. 74 (2015) 26–34.
[48] J.J. Thomas, The instantaneous apparent activation energy of cement hydration measured using a novel calorimetry-based method, J. Am. Ceram. Soc. 95 (2012) 3291–3296.